*Solar-Terrestrial Physics. 2022. Vol. 8. Iss. 3. P. 63–68. DOI: 10.12737/stp-83202210. © 2022 Nechaeva A.B., Zimovets I.V., Sharykin I.N. Published by INFRA-M Academic Publishing House*

UDC 523.9-1/-8
DOI: 10.12737/stp-83202210

Received February 28, 2022
Accepted June 23, 2022

# COMPARISON BETWEEN PROBABILITY DENSITY FUNCTIONS OF VERTICAL ELECTRIC CURRENT IN SOLAR ACTIVE REGIONS BASED ON HMI/SDO AND SOT/HINODE DATA

**A.B. Nechaeva**
*Space Research Institute RAS,*
*Moscow, Russia, nechaeva.ab@phystech.edu*

**I.V. Zimovets**
*Space Research Institute RAS,*
*Moscow, Russia, ivanzimovets@gmail.com*

**I.N. Sharykin**
*Space Research Institute RAS,*
*Moscow, Russia, ivan.sharykin@phystech.edu*

**Abstract.** Studying electric currents in solar active regions (AR) is an essential step in understanding solar activity in general and solar flares in particular. In this paper, we compare probability density functions of vertical electric current $PDF(|j_z|)$ in several active regions, using HMI/SDO and SOT/Hinode photospheric magnetic field data. We have established that in the AR parts which contain current structures with current density above the noise level ($|j_z|>9\cdot10^3$ statampere/cm$^2$) these functions are nearly identical. The main difference in *PDF*s for low (noise) $j_z \lesssim 9\cdot10^3$ statampere/cm$^2$ is due to differences in sensitivity of these two instruments. We have also found that the criterion of pixel selection from magnetic field strength is inapplicable, and the similarity between *PDF*s is determined by high $j_z$. For all $PDF(|j_z|)$ under study we have calculated the power law exponent of the *PDF* tail for the two instruments, which coincide within their errors for the current structures with current values above noise level. Thus there is no significant difference as to which instrument is used for analyzing probability density functions in high current parts of ARs where flares are localized.

**Keywords:** solar active regions, magnetic field, electric currents, solar flares.

## INTRODUCTION

When studying dynamic processes in solar active regions (ARs) including their flare productivity, consideration is usually given to the magnetic field because it is regarded as the main energy source. However, AR can also be considered in terms of electric currents as being related to the free magnetic energy. The electric current can be obtained from magnetic field data, using the Ampere—Maxwell law in differential

$$\mathrm{rot}H = \frac{4\pi}{c} j \quad (1)$$

or integral form

$$\oint_l Hdl = \frac{4\pi}{c} I. \quad (2)$$

At present, the magnetic field is routinely measured in the photosphere. Nonetheless, vector magnetograms are currently available only for one narrow (~100 km) layer, so the study on currents is mainly limited to their vertical component. Note that attempts are also made to estimate the horizontal electric current component [Severny, 1988; Puschmann et al., 2010; Fursyak, Abramenko, 2017; Nechaeva et al., 2021].

A number of studies have dealt with the relationship of electric current with AR's flare productivity (e.g., [Severny, 1988; Abramenko et al., 1990; Kontogiannis et al., 2017; Fursyak, 2018]). Zimovets et al. [2020a] have investigated the form of the probability density function of vertical electric current $PDF(|j_z|)$, its change caused by a flare in AR under study, and the relationship with some parameters of the AR. For a limited sample (48 events in 33 AR), defined earlier in [Zimovets et al., 2020b], no obvious changes in the $PDF(|j_z|)$ form before and after the flare as well as no relationship of the function parameters with the magnetic class of the AR considered were found. The study [Zimovets et al., 2020b] was based on vector magnetograms of the Helioseismic and Magnetic Imager instrument on board the Solar Dynamics Observatory (HMI/SDO) [Scherrer et al., 2012; Hoeksema et al., 2014]. The purpose of this work is to compare the probability density functions $PDF(|j_z|)$ derived from the data from two instruments — HMI/SDO and Solar Optical Telescope on board the Hinode spacecraft (SOT/Hinode) [Tsuneta et al., 2008]. In particular, we want to check whether the $PDF(|j_z|)$ constructed from SOT/Hinode data has the same form as that derived from HMI/SDO data, namely "bell-shaped" gaussian for low values $|j_z|$ and power-law tail for high values. Note that currents have previously been compared using data

from these two instruments in [Fursyak, 2018]; however, the probability density functions of vertical electric current and the conditions under which they coincide have not been addressed in that paper. The influence of the spatial resolution of an instrument on measured solar currents has been discussed in [Barnes, Leka, 2018].

## DATA ANALYSIS AND RESULTS

Using vector magnetograms for seven ARs, which produced flares of different importance (flare classes from C 1.0 to X 2.2), we have drawn vertical electric current maps from HMI/SDO and SOT/Hinode data. The magnetic field data was taken as close as possible in time to the flare, but in some cases the time between a magnetogram and the onset of a flare was as long as an hour due to the fact that SOT/Hinode has a large time step between cycles of data acquisition. In one AR (NOAA 11675), a magnetogram was taken twenty-four hours after the onset of a class C1.0 flare. ARs for the analysis have been selected from the Hinode Flare Catalog [Watanabe et al., 2012]. The list of ARs used for the analysis and flares under study is given in Table 1. The flare in AR 11675 is omitted from Table 1 since it occurred much before the magnetograms employed and there is no obvious connection between the calculated currents and this flare.

The vertical electric current $j_z$ maps have been drawn by the following algorithm: firstly, since the magnetic field data from the two instruments differs in pixel size, SOT/Hinode magnetograms (0.3 arcsec) were roughened to the resolution of HMI/SDO magnetograms (1 arcsec). Secondly, the magnetograms were superimposed pixel by pixel based on white-light data since the coordinates of the center of the SOT/Hinode magnetogram are not always correct. Note that SOT/Hinode magnetograms cover only part of the disk unlike magnetograms from HMI/SDO that observes the full solar disk. Then, from Ampere—Maxwell formula (1) we recalculated the magnetograms into vertical

Table 1

Active regions and flares in the vicinity of which (with respect to time) the analysis was performed

| Number of active region NOAA | Flare identifier | X-ray class of flare |
|---|---|---|
| 12790 | SOL2020-12-03T09:55 | C1.2 |
| 12673 | SOL2017-09-06T08:57 | X2.2 |
| 12665 | SOL2017-07-14T01:07 | M2.4 |
| 12297 | SOL2015-03-11T22:08 | C7.8 |
| 12080 | SOL2014-06-10T06:19 | C2.4 |
| 11675 | – | – |
| 11158 | SOL2011-02-15T10:02 | C1.0 |

electric current $j_z$ maps. For comparison, the calculations were made using integral formula (2). Further, for each AR we constructed and analyzed probability density functions of vertical current $PDF(|j_z|)$.

The procedure for constructing such functions is described in [Zimovets et al., 2020a] except that a non-standard normalization was applied. We adopt a more standard normalization such that a value in each bin of the $|j_z|$ histogram is equal to the number of pixels in the region considered with values in this bin (interval) divided by the total number of pixels in the region of interest and by the bin width. This corresponds to the estimated probability that a random variable (vertical current density) in this sample will have a value in a given range (bin) of values.

For convenience, Figure 1 presents magnetograms of two regions used to illustrate the results: NOAA 11675 and NOAA 11158.

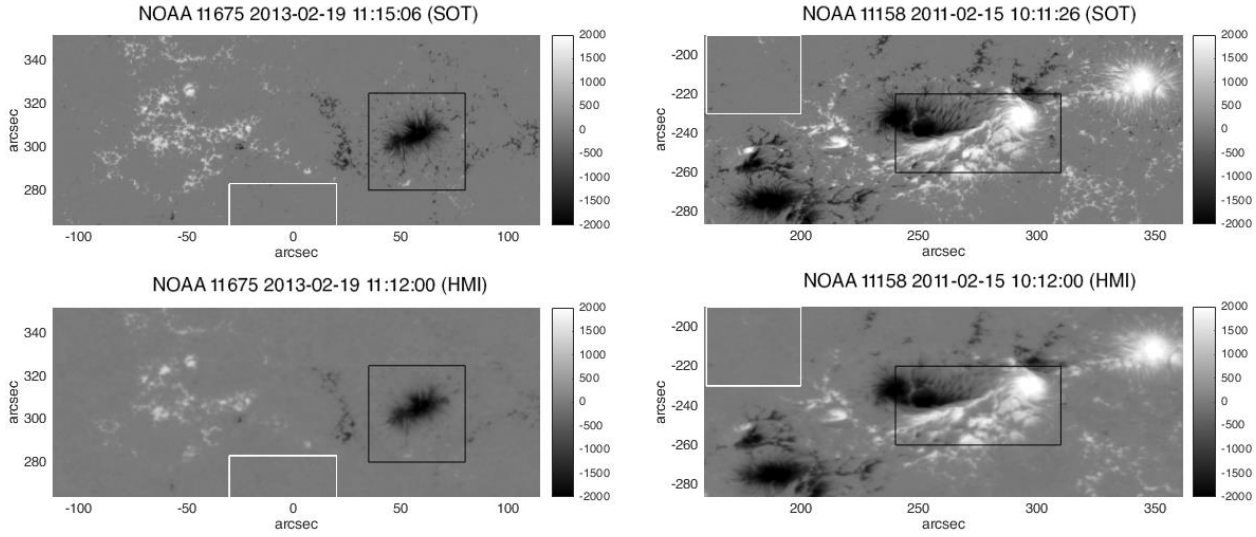


*Figure 1.* Magnetograms of the magnetic field vertical component $B_z$ in the photosphere for active regions NOAA 11675 (left) and NOAA 11158 (right) from SOT/Hinode (top panels) and HMI/SDO (bottom panels). Black and white rectangles indicate the AR parts used for the top and bottom panels of Figure 3 respectively

The resulting vertical current maps are given in Figure 2. AR NOAA 11675 is shown at the left; NOAA 11158, at the right. In the top panels are vertical electric current density maps derived from SOT/Hinode data; in the middle ones, from HMI/SDO data; the color scale is in SGS units $|j_z|$, i.e. statampere/cm$^2$. The bottom panels show probability densities of vertical electric current $PDF(|j_z|)$ in log-log scale (natural logarithm). Probability densities from SOT/Hinode data are represented in dark gray; from HMI/SDO data, in light gray. Different markers indicate the probability densities obtained from calculating $|j_z|$ by Ampere—Maxwell formulas in integral and differential forms. These probability densities can be seen to coincide, so there is no fundamental difference which way to use for calculating the current — integral or differential. It can also be observed that for the whole AR $PDF(|j_z|)$ slightly differs in form in the region $|j_z|<9\cdot10^3$ statampere/cm$^2$, which we call noise (see [Zimovets et al., 2020a]). This can be explained by the differences between background currents due to the different sensitivity of the instruments. Figure 3 shows $PDF(|j_z|)$ for different AR parts (marked in Figures 1 and 2 with black and white rectangles respectively): for the part with strong currents (top panel) and for the background AR part having generally only noise currents (bottom panel). Left panels display AR NOAA 11675; right panels, NOAA 11158. From noise current distributions we can see that they make the main difference in general $PDF(|j_z|)$ for the whole AR. Note that noise currents are located in the range of values to $|j_z|\sim9\cdot10^3$ statampere/cm$^2$, whereas the power-law tails of interest are above this value. Moreover, for NOAA 11158 this difference is initially smaller due to the fact that there are more pixels with high $|j_z|$ values in this region (see Figure 2).

For a more formal description of the similarity between distributions in the AR parts with strong currents, we fitted tails of the distributions by the power-law function $y=ax^b$ and compared the power-law exponents of the resulting distributions for the two instruments. Results of the fitting with errors are presented in Table 2. We can see that SOT/Hinode and HMI/SDO within error limits give similar results in those AR parts where strong currents are concentrated.

In addition, we have tested the hypothesis whether it is possible to determine the threshold value $B_{hor}$* of the horizontal magnetic field such that all AR pixels containing the

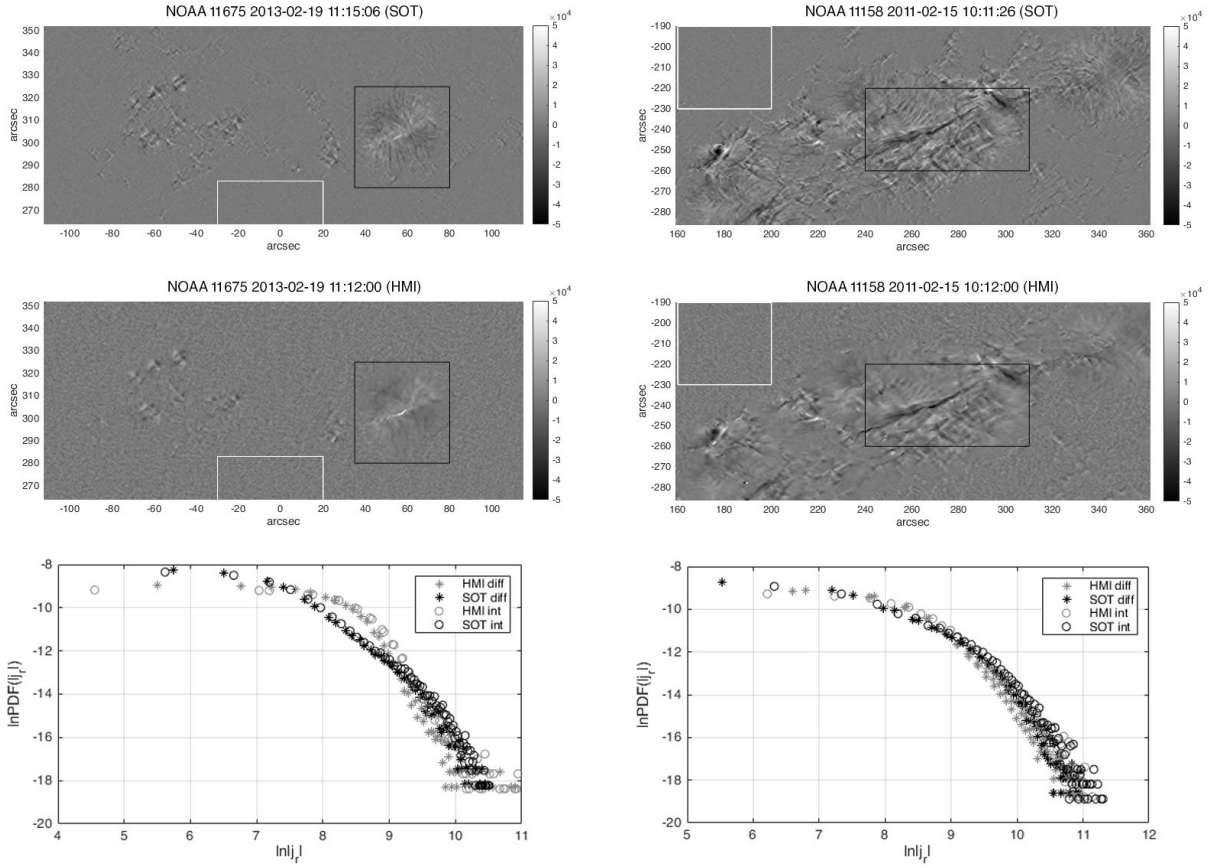


*Figure 2.* Vertical electric current density maps based on SOT/Hinode (top panels) and HMI/SDO (middle panels) data, as well as probability density functions $PDF(|j_z|)$ (bottom panels) for NOAA 11675 (left) and NOAA 11158 (right). Black and white rectangles in the top and middle panels mark the AR parts used for the top and bottom panels of Figure 3 respectively. In the bottom panel, asterisks and circles indicate the probability densities obtained by applying the Ampere—Maxwell law in dif-

ferential and integral forms to HMI/SDO (gray) and SOT/Hinode (black) magnetograms respectively

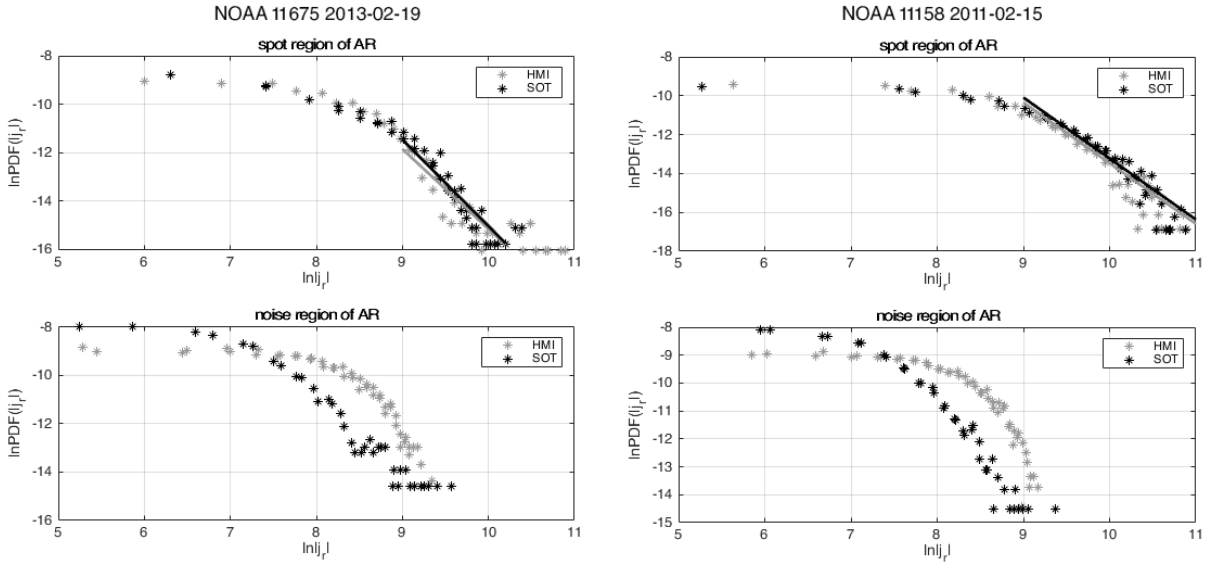


*Figure 3.* $PDF\left(\left|j_z\right|\right)$ for individual parts of NOAA 11675 (left panels) and NOAA 11158 (right panels), calculated from HMI/SDO (gray asterisks) and SOT/Hinode (black asterisks) data: the top panel is for the AR part with strong currents (black rectangle in Figure 2), straight lines are fittings of the power-law tail of distributions; the bottom panel is for the AR background part (white rectangle in Figure 2)

Table 2

Power-law $PDF\left(\left|j_z\right|\right)$ tail exponents (with errors) obtained by linear approximation (in loglog-scale) for all ARs considered

| Number of active region NOAA | Power-law tail exponent SOT/Hinode distributions | Power-law tail exponent HMI/SDO distributions |
|---|---|---|
| 12790 | –3.35±0.23 | –3.55±0.52 |
| 12673 | –2.51±0.23 | –2.79±0.29 |
| 12665 | –4.02±0.29 | –3.98±0.32 |
| 12297 | –3.32±0.32 | –3.02±0.24 |
| 12080 | –3.52±0.25 | –3.49±0.42 |
| 11675 | –3.56±0.62 | –3.29±0.40 |
| 11158 | –3.13±0.33 | –3.10±0.32 |

field $B_{hor}>B_{hor}$* would give the same distributions for the two instruments (it is the horizontal component of the magnetic field that is considered since it defines the vertical current according to Formulas (1) and (2)). To do this, we plotted the dependence of the residual sum of squares (RSS) normalized by the number of data-points on the strength of the horizontal magnetic field of cutoff. These dependencies are shown in Figure 4. As inferred from the plots for three of the regions considered, it is impossible to accurately determine the universal threshold $B_{hor}$* at which there is minimum RSS or RSS reaches a plateau.

## CONCLUSIONS

Analysis of seven flare ARs has revealed that the form of vertical electric current probability density functions is universal for SOT/Hinode and HMI/SDO: for low (background) $\left|j_z\right|$, the probability density is a "bell-shaped" gaussian; and for high ones, a power-law tail. In the AR background part, the $PDF\left(\left|j_z\right|\right)$ difference can be attributed to different sensitivity and spatial resolution of the instruments, whereas for those parts where currents of large amplitudes are concentrated the probability densities match well. For further analysis, we are interested only in power-law tails whose exponents coincide within error limits for data from the two instruments. The difference in the form of the current probability densities may also arise due to the fact that these two instruments use different spectral lines to construct magnetograms: 617.3 nm in HMI/SDO, and 630.2 nm in SOT/Hinode. The characteristic formation heights

of these lines in the classical atmosphere are estimated respectively as 270 km for HMI/SDO and 340 km and

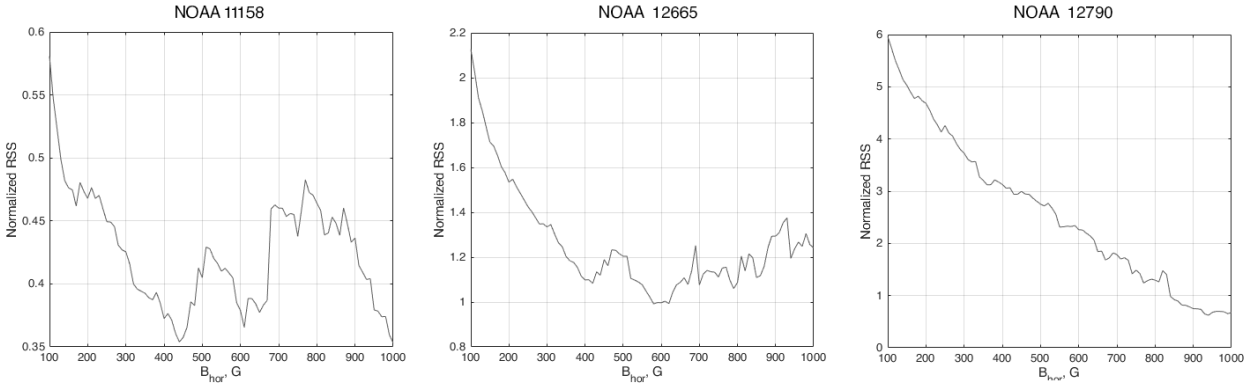


*Figure 4.* Residual sum of squares (RSS) normalized by the number of datapoints as a function of the absolute value of the horizontal magnetic field of cutoff for three ARs: NOAA 11158 (left panel), NOAA 12665 (middle panel), and NOAA 12790 (right panel)

260 km for SOT/Hinode [Löhner-Böttcher et al., 2019] since in the latter case there are two magnetically sensitive lines with different Lande factors. Yet it is unlikely that characteristics of vertical electric currents would differ significantly with such a small difference in heights (several times smaller than the size of magnetogram pixels). We can conclude that when using data from the less sensitive HMI/SDO instrument to analyze electric currents in the AR parts with strong currents we do not lose information as compared to the data from more sensitive SOT/Hinode. Moreover, pixels for analysis should be selected precisely by $|j_z|$, not by the magnetic field strength.

In the future, we plan to conduct a more detailed statistical analysis of $PDF(|j_z|)$ for a large sample of local flare AR parts, using HMI/SDO data, collected for almost the entire 24th solar cycle with 720 s time step for the full solar disk as opposed to SOT/Hinode data.

The work was financially supported by the Russian Science Foundation (Project No. 17-72-20134).

## REFERENCES

Abramenko V.I., Gopasiuk S.I., Ogir' M.B. The variety of solar flares revealed on the basis of the electric currents investigation. *Izvestiya Krymskoi Astrofizicheskoi Observatorii* [Bulletin of the Crimean Astrophysical Observatory]. 1990, vol. 81, pp. 8–13. (In Russian).

Barnes G., Leka K.D. Inferring currents from the Zeeman effect at the solar surface. *Electric Currents in Geospace and Beyond*. 2018. P. 81–91. (Geophys. Mon. Ser., vol. 235). DOI: 10.1002/9781119324522.ch5.

Fursyak Y.A. Vertical Electric currents in active regions: Calculation methods and relation to the flare index. *Geomagnetism and Aeronomy*. 2018, vol. 58, pp. 1129–1135. DOI: 10.1134/S0016793218080078.

Fursyak Y.A., Abramenko V.I. Possibilities for estimating horizontal electrical currents in active regions on the Sun. *Astrophys.* 2017, vol. 60, pp. 544–552. DOI: 10.1007/s10511-017-9505-6.

Hoeksema J.T., Liu Y., Hayashi K., Sun X., Schou J., Couvidat S., Norton A., Bobra M., Centeno R., Leka K.D., Barnes G., Turmon M. The Helioseismic and Magnetic Imager (HMI) vector magnetic field pipeline: Overview and performance. *Solar Phys.* 2014, vol. 289, pp. 3483–3530. DOI: 10.1007/s11207-014-0516-8.

Kontogiannis I., Georgoulis M.K., Park S.H., Guerra J.A. Non-neutralized electric currents in solar active regions and flare productivity. *Solar Phys*. 2017, vol. 292, p. 159. DOI: 10.1007/s11207-017-1185-1.

Löhner-Böttcher J., Schmidt W., Schlichenmaier R., Steinmetz T., Holzwarth R. Convective blueshifts in the solar atmosphere. III. High-accuracy observations of spectral lines in the visible. *Astron. Astrophys*. 2019, vol. 624, p. A57. DOI: 10.1051/0004-6361/201834925.

Nechaeva A.B., Sharykin I.N., Zimovets I.V., Chen F. Relationship between the horizontal gradient of the vertical magnetic field and the horizontal electric current on the photosphere in a model active region of the Sun. *Geomagnetism and Aeronomy.* 2021, vol. 61, pp. 956–963. DOI: 10.1134/S0016793221070148.

Puschmann K.G., Ruiz C.B., Martínez P.V. The electrical current density vector in the inner penumbra of a sunspot. *Astrophys. J. Lett.*. 2010, vol. 721, no. 1. DOI: 10.1088/2041-8205/721/1/L58.

Scherrer P.H., Schou J., Bush R.I., Kosovichev A.G., Bogart R.S., Hoeksema J.T., Liu Y., Duvall Jr. T.L., et al. The Helioseismic and Magnetic Imager (HMI) investigation for the Solar Dynamics Observatory (SDO). *Solar Phys.* 2012, vol. 275, pp. 207–227. DOI: 10.1007/s11207-011-9834-2.

Severny A.B. *Nekotorye problemy fiziki Solntsa*. [Some Problems in Solar Physics]. Moscow, *Nauka*, 1988. 224 p. (In Russian).

Tsuneta S., Ichimoto K., Katsukawa Y., Nagata S., Otsubo M., Shimizu T., Suematsu Y., Nakagiri M., et al. The Solar Optical Telescope for the Hinode Mission: An overview. *Solar Phys.* 2008, vol. 249, pp. 167–196. DOI: 10.1007/s11207-008-9174-z.

Watanabe K., Masuda S., Segawa T. Hinode Flare Catalogue. *Solar Phys.* 2012, vol. 279, pp. 317–322. DOI: 10.1007/s11207-012-9983-y.

Zimovets I.V., Nechaeva A.B., Sharykin I.N., Gan W.Q. Density distribution of photospheric vertical electric currents in flare-active regions of the Sun. *Astrophys.* 2020a, vol. 63, pp. 408–420. DOI: 10.1007/s10511-020-09645-0.

Zimovets I.V., Sharykin I.N., Gan W.Q. Relationships between photospheric vertical electric currents and hard X-ray sources in solar flares: Statistical study. *Astrophys. J.* 2020b, vol. 891, no. 2. DOI: 10.3847/1538-4357/ab75be.

*This paper is based on material presented at the 17th Annual*

*Conference on Plasma Physics in the Solar System, February 7–11, 2022, IKI RAS, Moscow*.

Original Russian version: Nechaeva A.B., Zimovets I.V., Sharykin I.N., published in Solnechno-zemnaya fizika. 2022. Vol. 8. Iss. 3. P. 68–73. DOI: 10.12737/szf-83202210. © 2022 INFRA-M Academic Publishing House (Nauchno-Izdatelskii Tsentr INFRA-M)

*How to cite this article*

Nechaeva A.B., Zimovets I.V., Sharykin I.N. Comparison between probability density functions of vertical electric current in solar active regions based on HMI/SDO and SOT/Hinode data. *Solar-Terrestrial Physics*. 2022. Vol. 8. Iss. 3. P. 63–68. DOI: 10.12737/stp-83202210.